J Appl Electrochem (2013) 43:367–374
DOI 10.1007/s10800-012-0515-0

ORIGINAL PAPER

Kinetic analysis of Li|Li^+ interphase in an ionic liquid electrolyte

Andrzej Lewandowski · Marcin Biegun · Maciej Galinski · Agnieszka Swiderska-Mocek

Received: 10 October 2012 / Accepted: 11 December 2012 / Published online: 19 December 2012

Abstract Kinetic analysis of the Li|Li^+ interphase in an electrolyte based on *N*-metyl-*N*-propylpyrrolidinium bis (trifluoromethanesulfon)imide ionic liquid (MPPyrrTFSI) and lithium bis(trifluoromethanesulfon)imide salt (LiTFSI) was performed. Li|electrolyte|Li and LiC_6|electrolyte|Li cells were galvanostatically charged/discharged in order to form solid electrolyte interphase (SEI) protecting layer. SEM images showed that the surface of both Li and LiC_6 anodes was covered with small particles. The fitting procedure of electrochemical impedance data taken at different temperatures gave three resistances (R_{el}, R_{SEI}, R_{ct}) and hence, three $\ln R = f(T^{-1})$ straight lines of different slopes. Specific conductivity and activation energy of the conduction process of the liquid electrolyte, were ca. $\sigma = 2.5$ mS cm^{-1} (at $T = 25.0$ °C) and $E_{el}^{\#} = 15$ kJ mol^{-1}. Activation energy for the conduction process in the SEI layer was ca. 56 kJ mol^{-1} in the case of the metallic lithium and 62 kJ mol^{-1} for the graphite anode. Activation energy of the charge transfer process, $E_{ct}^{\#}$, for Li and LiC_6 anodes was 71 and 65 kJ mol^{-1}, respectively. Analysis of literature data for different electrolytes suggests that the $E_{ct}^{\#}$ value for Li^+ reduction may be approximated by 57 ± 5 kJ mol^{-1}. Activation energy for the diffusion processes in the graphite electrode, detected from the Warburg coefficient, was ca 74 kJ mol^{-1}.

A. Lewandowski (✉) · M. Biegun · M. Galinski · A. Swiderska-Mocek
Faculty of Chemical Technology, Poznań University of Technology, Pl.Marie Sklodowskiej-Curie 5, 60 965 Poznan, Poland
e-mail: andrzej.lewandowski@put.poznan.pl

Keywords Ionic liquid · Lithium · Lithium-ion battery · SEI · EIS

1 Introduction

Solid electrolyte interphase (SEI) [1–9] formed on the lithium or lithiated graphite is of particular interest from the commercial and scientific point of view. The SEI layer is responsible for the transport of lithium cations between liquid electrolyte and a solid electrode and strongly influences both ohmic resistance of the system and kinetics of the charge transfer reaction. Conventional organic solvents (e.g. ethylene carbonate, propylene carbonate, dimethyl carbonate, etc.) used in commercial Li-ion cells, form an efficient SEI protective layer, however, they are flammable due to the relatively high vapor pressure. Room temperature ionic liquids (RTILs) have been studied as non-flammable electrolytes for Li-ion batteries [10–20]. Lithium and lithiated graphite corrode in contact with many liquid systems, including RTILs. Hence, solvent-free RTILs may be used as electrolytes provided that they contain additives able to form the SEI. The general aim of this was to study kinetics of Li^+ reduction on both metallic lithium and lithiated graphite from solvent-free electrolytes (RTILs). In such a case the reaction of the Li^+ cation desolvation at the electrolyte/SEI interphase does not take place. Vinylene carbonate (VC) has been selected as a SEI forming additive [11, 15, 16, 18–23]. This paper is a continuation of our studies of the Li|SEI|Li^+ system in ionic liquids. The previous paper reported kinetics of Li^+ reduction at metallic lithium from a room temperature ionic liquid (1-methyl-3-propylpiperidinium bis(trifluoromethanesulfon)imide) [24]. This investigations were extended to include a new ionic liquid and lithiated graphite anode.

2 Experimental

2.1 Materials

Lithium foil (0.75 mm thick, Aldrich), vinylene carbonate (VC, Aldrich), propylene carbonate (Aldrich), lithium bis(trifluoromethanesulfon)imide (LiTFSI, Fluka), graphite, (G, SL-20, BET surface area 6.0 $m^2\ g^{-1}$, Superior Graphite, USA), carbon black (CB, Alfa Aesar), poly(vinylidene fluoride) (PVdF, Fluka), *N*-methyl-2-pyrrolidinone (NMP, Fluka) were used as received from suppliers. *N*-methyl-*N*-propylpyrrolidinium bis(trifluoromethanesulfon) imide (MPPyrrTFSI), was obtained by the method described before [25]. Vinylene carbonate was stored at a max temperature of 8 °C to prevent its spontaneous polymerisation.

Liquid electrolyte (0.4 mol kg^{-1} LiTFSI in MPPyrrTFSI 90 wt% + VC 10 wt%) was obtained by dissolution of solid LiTFSI salt in a liquid mixture MPPyrrTFSI 90 wt% + VC 10 wt%. Solutions of electrolytes were prepared and cells were assembled in a glove box in the dry argon atmosphere using a thoroughly dried ionic liquid, and they were stored over metallic lithium as a drying medium.

2.2 Measurements

The size of graphite particles was determined with the Mastersizer 2000 (by Malvern Instruments Ltd., UK). The graphite (LiC_6) electrodes were prepared by casting graphite+CB+PVdF (ratio 85:10:5) slurry in *N*-methyl-2-pyrrolidinone (NMP, Fluka) on the copper current collector (diameter 12 mm) (NMP was evaporated in vacuum at 120 °C). The electrode contained typically 3.5–4.0 mg of the graphite. In the symmetric Li|Li^+ cells, two round-shaped lithium electrodes were cut off from the metallic-lithium foil (surface of 1.10 cm^2, ca. 44–45 mg) and separated by a glass micro-fibre GF/A separator (Whatman) soaked with the electrolyte and placed into a Swagelock® connecting tube. Cyclic voltammetry as well as electrochemical impedance spectroscopy (EIS) were performed with the use of the G750 Potentiostat/Galvanostat Measurements System (Gamry, USA). Impedance spectra were obtained using a frequency response analyser at a frequency range of 100 kHz–10 mHz, at the open circuit potential and amplitude of 10 mV. Deconvolution of spectra was performed with the Z-view software (Scribner Associates Inc., USA), according to the published procedures [4, 26]. Temperature dependence of electrolytes conductivity was measured with the use of a cell with platinum wire electrodes (cell constant: 4.8 cm^{-1}) thermostated through a water jacket. Scanning electron microscopy (SEM) of electrodes was performed with the Tescan Vega 5153 apparatus.

3 Results and discussion

3.1 Total impedance

Impedance spectra of symmetric Li|electrolyte|Li and LiC_6|electrolyte|Li systems (0.4 mol kg^{-1} LiTFSI in MPPyrrTFSI 90 wt% + VC 10 wt%) at different temperatures are shown in Figs. 1 and 2, respectively (where Z' and Z'' are real and imaginary parts of the impedance Z). Both

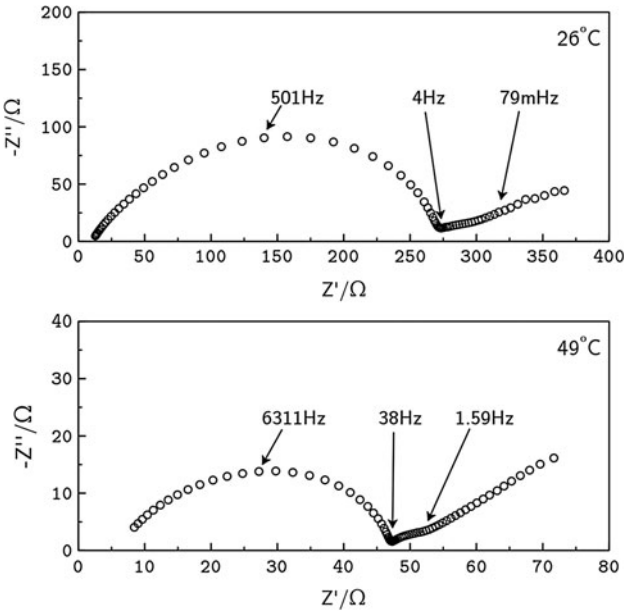

Fig. 1 EIS for the Li|SEI|Li^+ system in different temperatures

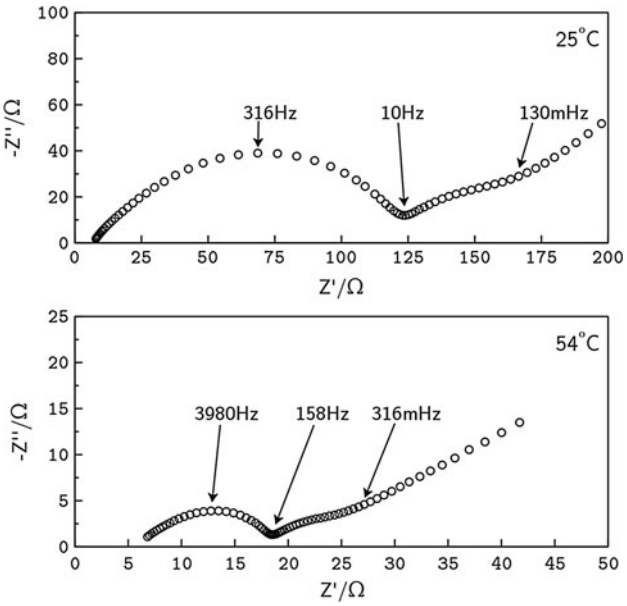

Fig. 2 EIS for the LiC_6|SEI|Li^+ system in different temperatures

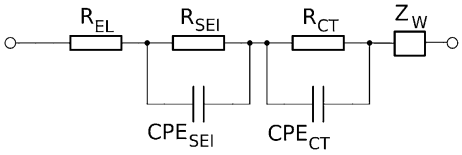

Fig. 3 Equivalent circuit used for impedance spectra deconvolution

cells were galvanostatically charged/discharged (1 mA, 5 min each cycle) in order to form electrochemically the SEI protecting layer. In the case of the graphite anode, EIS was taken when the electrode was intercalated. It can be seen that impedance spectra consist of a flat semicircle, followed by a short linear part. The latter low-frequency part, measured for the reduction of Li^+ on the metal-lithium anode is different in comparison to that characteristic of the LiC_6 anode, where the impedance due to lithium diffusion in graphite predominates. Total impedance of the Li|electrolyte is much higher in comparison to that characteristic of the LiC_6|electrolyte system. This may be due to the difference in electrode surface areas. While the surface area of the metallic lithium was ca. 1 cm^2, the corresponding geometrical surface area of graphite (ca. 3.5–4.0 mg, particle size 27.6 μm, surface area 6.0 $m^2\ g^{-1}$) was ca. 210–240 cm^2. The real graphite surface area was probably somewhat lower, as a part of it was covered with carbon black and the binder, and was not in contact with the electrolyte. The ratio of metallic-lithium and graphite electrodes real surface area may be approximated by two orders of magnitude (ca. 10^2). However, impedance of the LiC_6|electrolyte system is higher, in comparison to the Li|electrolyte one, by only one order of magnitude. The equivalent circuit used for impedance spectra deconvolution (Fig. 3) consisted of two *RC* elements describing resistance of SEI (R_{SEI}) and resistance of the charge transfer reaction (R_{ct}), in series with electrolyte resistance R_{el} and diffusion impedance represented by the Warburg element (Z_W). The fitting procedure of EIS data taken at different temperatures gave three resistances (R_{el}, R_{SEI}, R_{ct}) and hence, three $\ln R = f(T^{-1})$ straight lines of different slopes (Fig. 4) for both metallic-lithium and graphite anodes.

3.2 Electrolyte resistance R_{el}

Conductance of 0.4 mol kg^{-1} LiTFSI in MPPyrrTFSI 90 wt% + VC 10 wt% electrolyte, measured in the conductometric cell, was 2.5 mS cm^{-1} at $T = 25.0$ °C. The corresponding data for neat MPPyrrTFSI ionic liquid is somewhat lower, ca. 1.4 mS cm^{-1} at $T = 20$ °C [27]. This is probably due to the presence of molecular liquid (VC) in the LiTFSI + MPPyrrTFSI + VC electrolyte. Resistance of the electrolyte layer in the separator (ca. 0.2 mm thick) was ca. 5 Ω at room temperature. However, different structure of electrodes (metallic-Li or porous LiC_6) leads to difference in resistance of the electrolyte, especially at

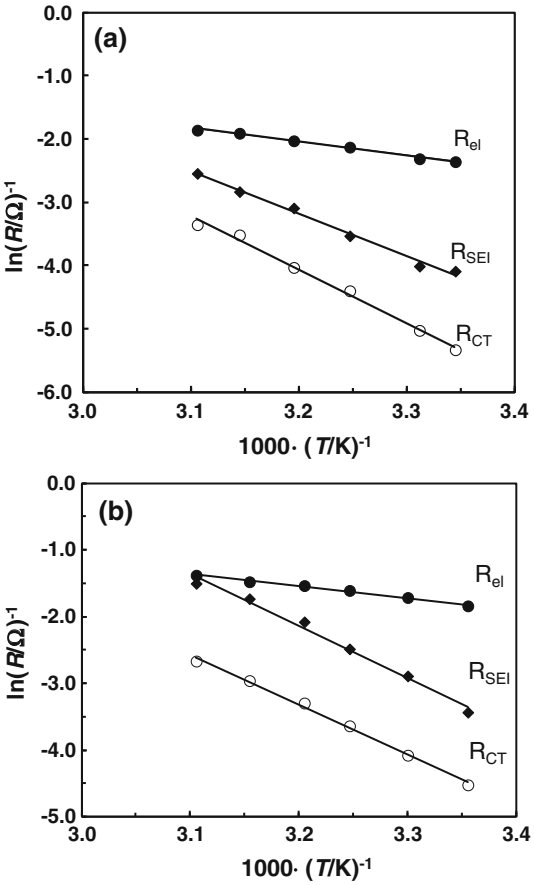

Fig. 4 Arrhenius plots for the **a** Li|SEI|Li^+ and **b** LiC_6|SEI|Li^+ systems

lower temperatures (Figs. 1, 2). Activation energy of the electrolyte conduction process, $E_{el}^{\#}$, determined from the slope of the Arrhenius $\ln R_{el} = f(T^{-1})$ plot, was ca. 15 kJ mol^{-1}.

3.3 SEI resistance R_{SEI}

Ohmic resistance associated with the first RC system (R_{SEI}) in the equivalent circuit (Fig. 3) is ca. 59 and 31 Ω at 298 K, for the Li|electrolyte and LiC_6|electrolyte systems, respectively. Both R_{SEI} resistances are of the same order, but the surface area differs by two orders of magnitude. While the metallic lithium surface area is ca. 1 cm^2, the geometrical surface area of the graphite and hence the area of the SEI is much higher (210–240 cm^2). R_{SEI} resistances of lithium and graphite electrodes decreased with temperature increase (49 °C) to ca. 12.7 and 4.5 Ω, respectively. Activation energy for the conduction process in the SEI layer is 56 kJ mol^{-1} in the case of metallic lithium and 62 kJ mol^{-1} for the graphite anode.

SEM images of the metallic lithium and graphite electrodes are shown in Figs. 5 and 6, respectively. It can be seen that after galvanostatic charging/discharging, the

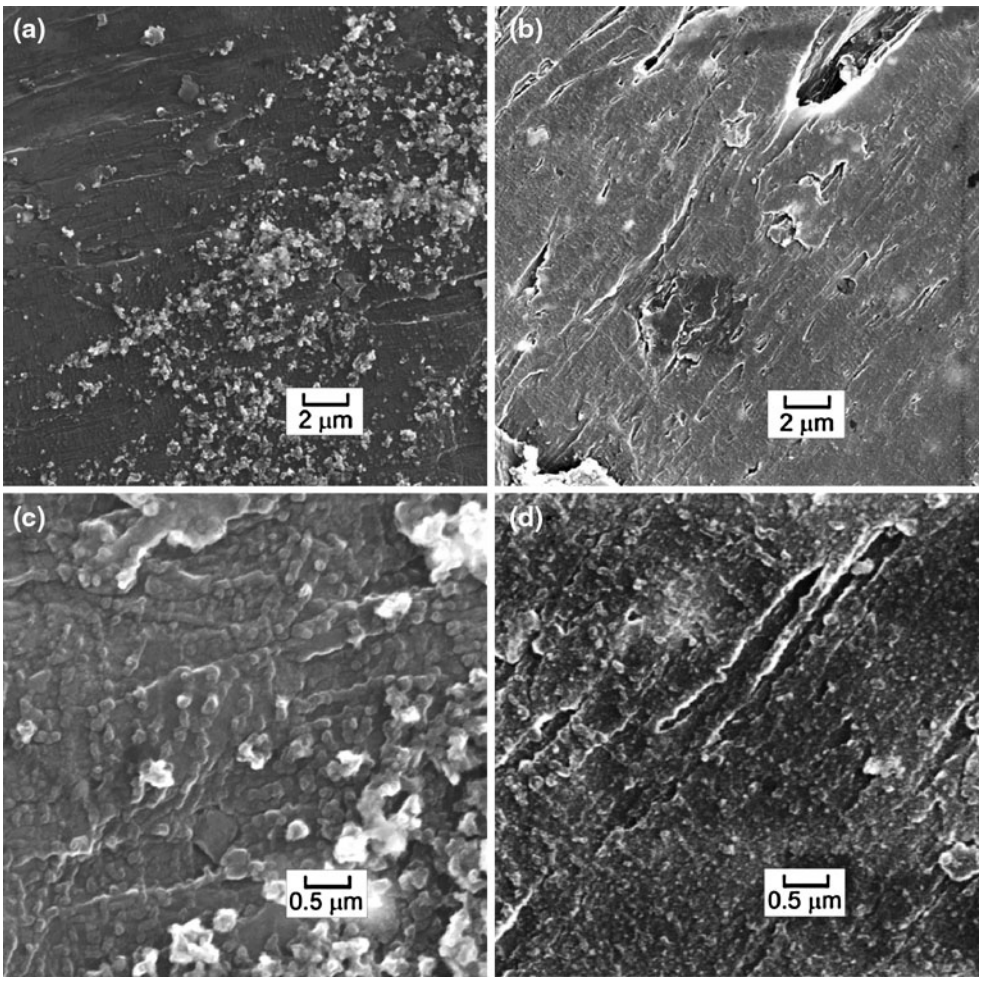

Fig. 5 SEM images of metallic lithium anode after galvanostatic charging/discharging/charging cycles performed at different temperatures 22.0 °C (**a**, **c**) and 55.0 °C (**b**, **d**). *Electrolyte* MPPyrrTFSI+LiTFSI+VC (10 wt%)

surface of both materials is covered with small particles. Moreover, a difference can be seen in morphology between samples cycled at different temperatures. In both cases (Li and G) the diameter of particles formed at lower temperatures (22 °C) is higher (ca. 0.2 μm) in comparison to those deposited at higher temperatures (55 °C). In addition, the graphite structure seems to be slightly exfoliated when galvanostatically charged/discharged at a higher temperature (55 °C). Taking into account the fact that the thickness of the SEI layer is low (up to 100 nm [8]), R_{SEI} values of the order of 10–100 Ω (with the surface area of 1 cm^2) indicate very low SEI conductivity of ca. $\sigma_{SEI} \approx 10^{-5}/(10–100) \approx 10^{-6}–10^{-7}$ S cm^{-1}.

3.4 Charge transfer resistance R_{ct}

The SEI layer has not only a protective function, but it also influences the kinetics of the charge transfer process, which takes place at the interphase between two solids: anode|SEI. The value of the charge transfer resistance, R_{ct}, for Li^+ reduction (at 25 °C) on metallic lithium was ca. 206 Ω and the corresponding value for the graphite electrode was 92 Ω. Approximating the metallic lithium surface by its geometric value, the exchange current density may be calculated from the R_{ct} according to:

$$j_o = \frac{RT}{F}\frac{1}{R_{ct}} \quad (1)$$

Finally, j_o for Li^+ reduction at lithium is $j_o \approx 0.025/206$ A $cm^{-2} = 1.24 \times 10^{-4}$ A cm^{-2}. It was difficult to estimate the real surface area of the graphite electrode (Fig. 6) and the corresponding exchange current density for the LiC_6|electrolyte system was not calculated. Activation energy $E_{ct}^{\#}$ for the charge transfer process, detected from the $\ln R_{ct} = f(T^{-1})$ plot (Fig. 4) for the lithium and graphite electrodes was 71 and 65 kJ mol^{-1}, respectively. The corresponding values measured for both Li and LiC_6 anodes, in a number of different electrolytes (Table 1), may be approximated by $E_{ct}^{\#} = 57 \pm 5$ kJ mol^{-1} (except for the LiC_6|($LiClO_4$ in DMC) and LiC_6|($LiPF_6$ in EC) systems) [24–31].

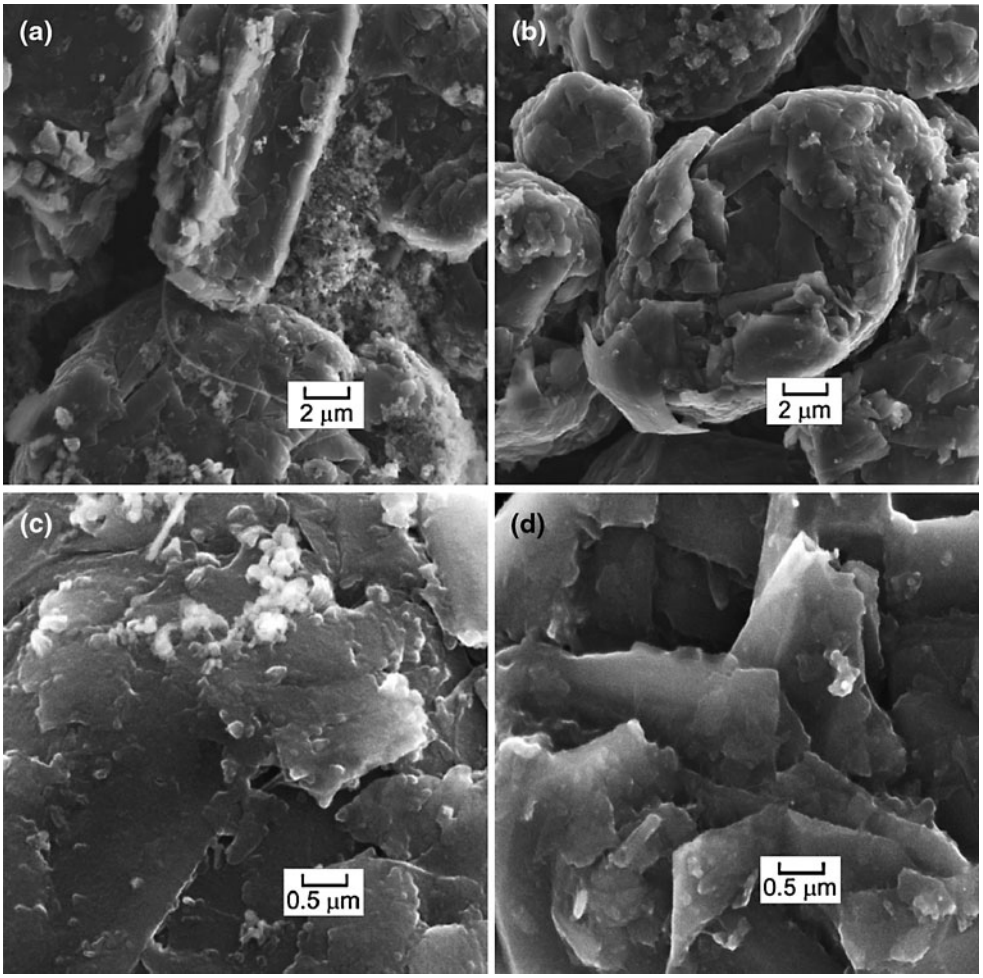

Fig. 6 SEM images of graphite anode after galvanostatic charging/discharging/charging cycles (intercalated state) performed at different temperatures 22.0 °C (**a**, **c**) and 55.0 °C (**b**, **d**). *Electrolyte* MPPyrrTFSI+LiTFSI+VC (10 wt%)

Note that the charge transfer reaction takes place at the junction between two solid phases Li|SEI or LiC_6|SEI and not between liquid electrolyte and the solid electrode. Consequently, solvation or desolvation of the lithium ion should not influence the charge transfer process. This may explain the relatively high independence of activation energy from the liquid electrolyte composition.

3.5 Diffusion impedance

The line which can be seen at EIS plots at the low-frequency region, is due to the diffusion of the electro-active species. The slope is not exactly 45°, however, both Z' and Z'' are linear functions of the angular frequency square root, according to the Warburg model. Hence, the diffusion process was approximated by the Warburg equation:

$$Z_W = \frac{A_W}{\sqrt{\omega}} - i\frac{A_W}{\sqrt{\omega}} \quad \text{and} \quad |Z_W| = \sqrt{2}\frac{A_W}{\sqrt{\omega}} \tag{2}$$

where i is the imaginary unit and A_W is the Warburg constant. The constant A_W depends both on the bulk concentration c and diffusion coefficient D of the diffusing electro-active species:

$$A_W = \frac{RT}{F^2 A\sqrt{2}}\left(\frac{1}{\sqrt{D_c}}\right) \tag{3}$$

The coefficient A_W can be determined from the slope of the $Z = f(\omega^{-1/2})$ plot. Both the real and imaginary parts of Z are plotted versus $\omega^{-1/2}$ (Fig. 7). The lines are approximately parallel, the slope should be equal to A_W. The line for the imaginary component should intersect the Z'' axis at zero, while the intercept (the Z' axis) for the real component is R_{ct}. The Warburg coefficient for the LiC_6 electrode at $T = 30$ °C was ca. $A_W = 10\ \Omega\ s^{-1/2}$ (Fig. 7), however, the diffusion coefficient rather cannot be estimated from Eq. (3), as Li^+ cations are reduced from the SEI layer and not from the liquid electrolyte. Consequently, the concentration c of Li^+ in SEI, necessary for calculations, is not known. According to the literature data

Table 1 Activation energy, $E_{ct}^{\#}$ of the charge transfer process of lithium-ion reduction

Electrode	Electrolyte	$E_{ct}^{\#}$/kJ mol^{-1}	References
LiC_6	$LiPF_6$/EMC	53.1	[29, 30]
LiC_6	$LiPF_6$/DMC	57.5	[29, 30]
LiC_6	$LiBF_4$/DMC	58.5	[29, 30]
LiC_6	$LiBF_4$/EC	53.1	[30]
LiC_6	$LiPF_6$/EC	71.1	[29]
LiC_6 (HOPG)	$LiClO_4$/DMC	40	[31]
LiC_6 (HOPG)	Li ClO_4/EC:DMC 1:9	55	[31]
LiC_6 (HOPG)	Li ClO_4/EC:DMC 1:1	58	[31]
LiC_6 (HOPG)	Li ClO_4/EC:DMC 1:1 + VC 3 %)	56	[31]
LiC_6 (HOPG)	Li ClO_4/EC:DMC 1:1 + PFS 3 %)	56	[31]
LiC_6 (HOPG)	Li ClO_4/DMC + PFS 3 %)	52	[31]
$Li_4Ti_5O_{12}$	$LiPF_6$/EC(0-70 %/DMC)	50-54	[32]
Li	LiTFSI/MPPipTFSI + VC (10 %)	62	[24]
Li	LiTFSI/MPPyrrTFSI + VC (10 %)	56	This study
LiC_6	LiTFSI/MPPyrrTFSI + VC (10 %)	62	This study

HOPG highly oriented pyrolytic graphite, *PFS* 2,3,4,5,6-pentafluorostyrene, *MPPip* methylpropyl piperidinium cation, *EC* ethylene carbonate, *DMC* dimethylcarbonate, *EMC* ethylmethyl carbonate

Li diffusion coefficient in carbon materials at room temperature is between 10^{-9} and 10^{-11} cm^2 s^{-1} [11].

Equation 3 may be rewritten into the following form:

$$\ln D = \ln \alpha - 2 \ln \frac{A_W}{T} \tag{4}$$

where α is a constant determined by the bulk concentration c of Li^+ cations and the area A across which Li^+ diffuse.

On the other hand, the temperature dependence of the diffusion coefficient D may be approximated by the Arrhenius-type equation:

$$\ln D = \ln D_o - \frac{E_D^{\#}}{R} \frac{1}{T} \tag{5}$$

A combination of Eqs. (4) and (5) leads to a linear expression $\ln(A_W/T) = f(T^{-1})$, which slope indicates the activation energy $E_D^{\#}$ of the diffusion process:

$$\ln \frac{A_W}{T} = \beta - \frac{E_D^{\#}}{2R} \frac{1}{T} \tag{6}$$

where β is a constant determined by D_o, A and c values.

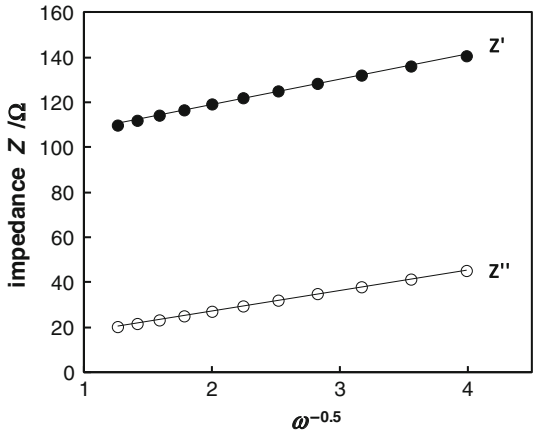

Fig. 7 Dependency of the angular frequency on the real (Z') and imaginary (Z'') parts of the impedance at low-frequency region for the LiC_6|MPPyrrTFSI+LiTFSI system. $T = 30$ °C

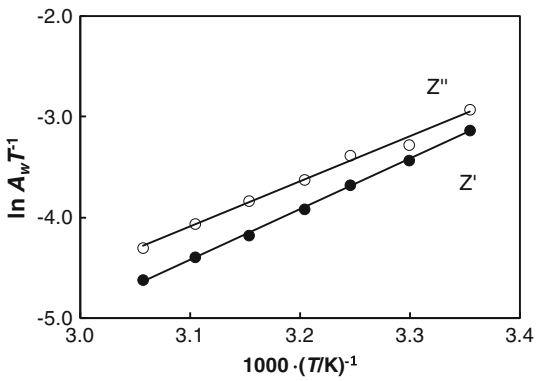

Fig. 8 Dependency of the $\ln A_w T^{-1}$ (calculated from Z'' and Z') as a function of the inverse of the temperature for the LiC_6|MPPyrrTFSI+LiTFSI system

Activation energy, $E_D^{\#}$, for the LiC_6 (Fig. 8) electrode, determined from the $\ln(A_W/T) = f(T^{-1})$ function is ca 74 kJ/mol.

4 Conclusions

1. Li|electrolyte|Li and LiC_6|electrolyte|Li cells were galvanostatically charged/discharged in order to form the SEI protecting layer. SEM images showed that the surface of both Li and LiC_6 anodes was covered with small particles. In addition, graphite structure seemed to be slightly exfoliated when galvanostatically charged/discharged at a higher temperature (55 °C).
2. Impedance spectra (EIS) consisted of a flat semicircle, followed by a short linear part. The fitting procedure of EIS data taken at different temperatures gave three resistances (R_{el}, R_{SEI}, R_{ct}) and hence, three $\ln R = f(T^{-1})$ straight lines of different slopes.
3. Specific conductivity and activation energy of the conduction process of the liquid electrolyte were ca. $\sigma = 2.5$ mS cm^{-1} (at $T = 25.0$ °C) and $E_{el}^{\#} = 15$ kJ mol^{-1}, respectively.
4. Activation energy for the conduction process in the SEI layer was ca. 56 kJ mol^{-1} in the case of the metallic lithium and 62 kJ mol^{-1} for the graphite anode.
5. The activation energy of the charge transfer process, $E_{ct}^{\#}$, for both Li and LiC_6 anodes were 71 and 65 kJ mol^{-1}. Analysis of literature data for different electrolytes suggests that the $E_{ct}^{\#}$ value may be approximated by $E_{ct}^{\#} = 57 \pm 5$ kJ mol^{-1}.
6. Activation energy, $E_D^{\#}$, for the diffusion processes in the graphite electrode, detected from the Warburg coefficient, was ca 74 kJ mol^{-1}.

Acknowledgments Support of Grant 31-242/12 DS-PB is gratefully acknowledged.

References

1. Peled E (1979) The electrochemical behavior of alkali and alkaline earth metals in nonaqueous battery systems—the solid electrolyte interphase model. J Electrochem Soc 126:2047–2051
2. Rahner D, Machill S, Siury K (1997) Passivity of lithium in organic solvents. J Power Sour 68:69–74
3. Yazami R, Touzain P (1983) A reversible graphite-lithium negative electrode for electrochemical generators. J Power Sour 9:365–371
4. Dey A (1977) Lithium anode film and organic and inorganic electrolyte batteries. Thin Solid Films 43:131–171
5. Zaban A, Zinigrad E, Aurbach D (1996) Impedance spectroscopy of Li electrodes. 4. A general simple model of the Li-solution. Interphase in polar aprotic systems. J Phys Chem 100:3089–3101
6. Aurbach D (2000) Review of selected electrode–solution interactions which determine the performance of Li and Li ion batteries. J Power Sour 89:206–218
7. Edstrom K, Herstedt M, Abraham DP (2006) A new look at the solid electrolyte interphase on graphite anodes in Li-ion batteries. J Power Sour 153:380–384
8. Bryngelsson H, Stjerndahl M, Gustafsson T, Edstrom K (2007) How dynamic is the SEI? J Power Sour 174:970–975
9. Peled E, Golodnitsky D (2004) SEI on lithium. In: Balbuena PB, Wang Y (eds) Lithium-ion batteries, solid-electrolyte interphase. Imperial College Press, London, pp 16–39
10. Holzapfel M, Jost C, Novak P (2004) Stable cycling of graphite in an ionic liquid based electrolyte. Chem Commun 2004:2098–2099
11. Galinski M, Lewandowski A, Stepniak I (2006) Ionic liquids as electrolytes. Electrochim Acta 51:5567–5580
12. Sato T, Maruo T, Marukane S, Takagi K (2004) Ionic liquids containing carbonate solvent as electrolytes for lithium ion cell. J Power Sour 138:253–261
13. Zheng H, Jiang J, Abe T, Ogumi Z (2006) Electrochemical intercalation of lithium into a natural graphite anode in quaternary ammonium-based ionic liquid electrolytes. Carbon 44:203–210
14. Jin J, Li HH, Wei JP, Bian XK, Zhou Z, Yan J (2009) Li/$LiFePO_4$ batteries with room temperature ionic liquid as electrolyte. Electrochem Commun 11:1500–1503
15. Holzapfel M, Jost C, Prodi-Schwab A, Krumeich F, Wursig A, Buqa H, Novak P (2005) Stabilisation of lithiated graphite in an electrolyte based on ionic liquids: an electrochemical and scanning electron microscopy study. Carbon 43:1488–1498
16. Guerfi A, Dontigny M, Charest P, Petitclerc M, Lagace P, Vijh A, Zaghib K (2010) Improved electrolytes for Li-ion batteries: mixtures of ionic liquid and organic electrolyte with enhanced safety and electrochemical performance. J Power Sour 195: 845–852
17. Byrne N, Howlett PC, MacFarlane DR, Forsyth M (2005) The Zwitterion effect in ionic liquids: towards practical rechargeable lithium-metal batteries. Adv Mater 17:2497–2501
18. Lewandowski A, Świderska-Mocek A (2009) Properties of the lithium and graphite–lithium anodes in *N*-methyl-*N*-propylpyrrolidinium bis(trifluoromethanesulfonyl)imide. J Power Sources 194: 502–507
19. Abe K, Miyoshi K, Hattori T, Ushigoe Y, Yoshitake H (2008) Functional electrolytes: synergetic effect of electrolyte additives for lithium-ion battery. J Power Sour 184:449–455
20. Seki S, Kobayashi Y, Miyashiro H, Ohno Y, Mita Y, Terada N, Charest P, Guerfi A, Zaghib K (2002) Compatibility of *N*-methyl-*N*-propylpyrrolidinium cation room-temperature ionic liquid electrolytes and graphite electrodes. J Phys Chem C 112:16708–16713
21. Aurbach D, Gamolsky K, Markovsky B, Gofer Y, Schmidt M, Heider U (2002) On the use of vinylene carbonate (VC) as an additive to electrolyte solutions for Li-ion batteries. Electrochim Acta 47:1423–1439
22. Fu Y, Chen C, Qiu C, Ma X (2009) Vinyl ethylene carbonate as an additive to ionic liquid electrolyte for lithium ion batteries. J Appl Electrochem 39:2597–2603
23. Sun XG, Dai S (2010) Electrochemical investigations of ionic liquids with vinylene carbonate for applications in rechargeable lithium ion batteries. Electrochim Acta 55:4618–4626
24. Lewandowski A, Biegun M, Galinski M (2012) Kinetics of Li^+ reduction in 1-methyl-3-propylpiperidinium bis(trifluoromethylsulfonyl) imide room temperature ionic liquid. Electrochim Acta 63:204–208
25. Appetecchi GB, Scaccia S, Tizzani C, Alessandrini F, Passerini D (2006) Synthesis of hydrophobic ionic liquids for electrochemical applications. J Electrochem Soc 153: A1685–A1691
26. Pelled E, Golodnitsky D, Ardel G (1997) Advanced Model for Solid Electrolyte Interphase Electrodes in Liquid and Polymer Electrolytes. J Electrochem Soc 144:L208–L210

27. Barisci JN, Walace GG, MacFarlane DR, Baughman RH (20004) Investigation of ionic liquids as electrolytes for carbon nanotube electrodes. Electrochem Commun 6:22-27
28. Xu K, Lam Y, Zhang SS, Jow TR, Curtis TB (2007) Solvation Sheath of Li^+ in Nonaqueous Electrolytes and Its Implication of Graphite/Electrolyte Interface Chemistry. J Phys Chem C 111: 7411–7421
29. Xu K (2007)"Charge-Transfer" Process at Graphite/Electrolyte Interface and the Solvation Sheath Structure of Li^+ in Nonaqueous Electrolytes. J Electrochem Soc 154:A162-A167
30. Yamada Y, Iriyama Y, Abe T, Ogumi Z (2009) Kinetics of lithium ion transfer at the interface between graphite and liquid electrolytes: effects of solvent and surface film. Langmuir 25:12766–12770
31. Xu K, von Cresce A, Lee U (2010) Differentiating contributions to "ion transfer" barrier from interphasial resistance and Li^+ desolvation at electrolyte/graphite interface. Langmuir 26:11538–11543
32. Churikov AV, Volgin MA, Pridatko KI (2002) On the determination of kinetic characteristics of lithium intercalation into carbon. Electrochim Acta 47:2857–2865